Disruption of the Heme Iron−Proximal Histidine Bond Requires Unfolding of Deoxymyoglobin†

Qun Tang,‡ William A. Kalsbeck,‡ John S. Olson,§ and David F. Bocian*,‡

Department of Chemistry, University of California, Riverside, California 92521-0403, and Department of Biochemistry and Cell Biology and the W. M. Keck Center for Computational Biology, Rice University, Houston, Texas 77251-1892

Received December 2, 1997; Revised Manuscript Received February 26, 1998

ABSTRACT: The unfolding behavior of 10 different distal heme pocket mutants of sperm whale deoxymyoglobin (deoxyMb) has been investigated. The effects of distal histidine (His 64) replacement were the primary focus; however, mutations at Leu 29, Val 68, and Ile 107 were also examined. Formation of the spectroscopically distinguishable heme intermediate (I′) of deoxyMb was tracked as a function of pH and guanidinium chloride (GdmCl) concentration. The appearance of this intermediate signals cleavage of the iron−proximal histidine (His 93) bond. The key observations are as follows. (1) None of the distal heme pocket mutations investigated alter the nature of the heme intermediates that are formed under low pH unfolding conditions. (2) Unfolding of deoxyMb at high concentrations of GdmCl proceeds through the same heme intermediates that occur under low pH conditions. (3) The rate of the iron−histidine bond cleavage in an acidic medium is dramatically slowed when large hydrophobic residues (Leu and Phe) replace the distal histidine, whereas there is little correlation between the polarity of the residue at position 64 and the rate of denaturation by GdmCl. (4) However, apolar residues at position 64 enhance significantly the equilibrium resistance of deoxyMb to iron−histidine bond cleavage under both low pH and high GdmCl unfolding conditions. There is a direct correlation between the equilibrium pH and GdmCl values for maximum intermediate formation and the stabilities of the corresponding apoproteins. Collectively, these observations suggest that substantial unfolding of deoxyMb is required for Fe(II)−His 93 bond cleavage. Unlike the situation for aquometMb, heme loss from deoxyMb is not driven by protonation of the proximal histidine ligand. Instead, the process is mediated by more global unfolding of the protein that leads to solvation of the prosthetic group.

Apomyoglobin (apoMb)[1] and apohemoglobin exhibit extremely high affinities for iron protoporphyrin IX which serves as the O_2 binding prosthetic group in the proteins (*1*, *2*). The incorporation of heme in turn significantly stabilizes the holoprotein with respect to the apo form (*3*−*7*). Accordingly, the development of general models of holoprotein stability requires a detailed understanding of both the interactions between the heme and globin and the factors that influence heme loss and protein denaturation. Understanding these properties is also important for developing novel extracellular recombinant heme proteins that exhibit sufficiently high stability and expression yields to serve as effective O_2 delivering systems (i.e., blood substitutes).

Recently, Hargrove, Olson, and co-workers reported a series of studies on wild-type and genetically modified Mbs aimed at determining the factors that influence the association/dissociation rates of the heme group and the overall stability of the protein (*2*, *5*, *8*, *9*). The association studies utilized both ferrous (heme) and ferric (hemin) iron porphyrins, whereas the heme dissociation and protein stability studies primarily utilized metMb, which contains ferric iron porphyrin. The salient features that emerged from these studies are as follows. (1) The association rate constant for heme/hemin is relatively independent of protein structure (*2*). (2) Bound hemin stability is primarily determined by hydrophobic interactions between the apolar protein residues and the porphyrin ring augmented by the iron−proximal histidine bond and hydrogen bonding interactions between distal residues and hemin-bound water (*8*). (3) The stability of metMb is primarily determined by hemin affinity and does not directly correlate with the apoprotein stability (*5*). Collectively, these observations establish the foundation for understanding the complex interplay of factors that mediate prosthetic group−globin interactions and holoprotein stability.

The physiologically active deoxy form of Mb contains heme rather than hemin. Nevertheless, studies of deoxyMb unfolding are much more limited than those on metMbs. Investigations of wild-type and selected mutant deoxyMbs have revealed that the deoxy forms are ∼60 times more stable than the met analogues (*5*). The enhanced resistance

† This work was supported by U.S. Public Health Service Grants GM-36243 (D.F.B.), GM-35649 (J.S.O.), and HL-47020 (J.S.O.); Grant C-612 from the Robert A. Welch Foundation (J.S.O.); and the W. M. Keck Foundation (J.S.O.).

‡ University of California.

§ Rice University.

[1] Abbreviations: CCD, charge-coupled device; GdmCl, guanidinium chloride; I′, intermediate of partially unfolded deoxymyoglobin characterized by a 426-nm heme Soret absorption maximum; Mb, myoglobin; N, native form of myoglobin; RR, resonance Raman; SW, sperm whale; U, unfolded form of myoglobin that occurs below pH 2.0; U′, intermediate form of partially unfolded deoxymyoglobin characterized by a 383-nm heme Soret absorption maximum.

S0006-2960(97)02941-3 CCC: $15.00
Published on Web 04/22/1998

to heme loss and the concomitant increased stability of the protein result from the large increase in iron−histidine bond strength that occurs upon reduction of the metal ion from the ferric to the ferrous oxidation state (*10*, *11*). Consequently, for deoxyMbs, the iron−histidine bond becomes nearly as important as porphyrin−protein hydrophobic interactions in determining the heme affinity and protein stability (*5*).

The optical and vibrational signatures of the heme group of deoxyMb provide a detailed picture of the structural characteristics of the heme and its interaction with the protein matrix (*12*−*15*). These spectroscopic signatures also afford the opportunity for tracking the structure of the heme during unfolding of the holoprotein. In particular, the acid unfolding of deoxyMb from the native (N) form to the unfolded (U) form proceeds through at least two spectroscopically distinct heme intermediates (*16*−*26*). The first intermediate (I′-form) occurs in the pH ∼3.5−4.5 range and is characterized by a Soret maximum near 426 nm (compared with 434 nm for the N-form) (*21*−*25*). In the I′-form, the iron−histidine bond is broken; however, the heme is five-coordinate due to relatively tight binding of a water molecule (*23*, *24*). The I′-form is observed in both equilibrium pH titrations and pH jump experiments. The kinetics of I′-intermediate formation have been successfully accounted for using a three-state linear free-energy model which incorporates the effects of both pH and ionic strength (*25*). The second spectroscopically distinct heme intermediate (U′-form) occurs in the pH 2.6−3.5 range and exhibits a Soret maximum near 383 nm. Although the spectroscopic signatures of the U′-form are qualitatively similar to those of aggregated heme which has dissociated from the globin, certain spectral differences led Champion and co-workers to suggest that this species is a true intermediate wherein the heme remains associated with the protein (*26*). The U′-intermediate is observed in both metMb and deoxyMb (*24*, *26*). In contrast, the I′-intermediate has only been detected in deoxyMb (*24*).

The occurrence of spectroscopically distinct heme intermediates during the acid unfolding of deoxyMb affords the opportunity for investigating how specific properties of the heme pocket influence the lability of the iron−histidine bond and the stability of the ferrous holoprotein. Consequently, we examined the acid unfolding behavior of 10 different distal heme pocket mutants of deoxyMb. The effects of distal histidine (His 64) replacement were the primary focus of the studies; however, the effects of mutations at Leu 29, Val 68, and Ile 107 were also investigated. The various mutant myoglobins were chosen because they exhibit a wide range of heme affinities and apoprotein stabilities (*5*, *8*, *9*). The group also includes proteins in which a distal heme pocket water molecule is present (native/wild-type deoxyMb (*12*, *27*, *28*)) or absent (mutants with hydrophobic replacements at position 64 (*29*−*33*)). All of the spectroscopic studies track the formation of the I′-intermediate of deoxyMb. This intermediate was targeted because its formation signals cleavage of the iron−histidine bond (*23*, *24*), which is a key step determining heme dissociation and protein stability (*5*, *8*).

A parallel series of guanidinium chloride (GdmCl) unfolding studies were performed on wild-type and selected mutant deoxyMbs. These studies were initiated to determine whether the I′-intermediate is unique to the low pH environment, wherein the proximal histidine is protonated, or whether the intermediate is general to the unfolding process. Collectively, the studies elucidate the properties of the heme pocket that control iron−histidine bond lability, mediate heme dissociation, and inhibit holoprotein denaturation.

MATERIALS AND METHODS

General Sample Preparation Procedures. Wild-type sperm whale (SW) Mb (H64H) and the mutants at positions 29, 64, 68, and 107 were prepared as described by Hargrove et al. (*9*). Recombinant wild-type Mb differs from the native protein. A methionine initiator is appended to the N-terminus of the recombinant protein, and Asp 122 is mutated to Asn. All buffers were prepared from reagent grade materials. Horse skeletal muscle Mb was purchased from Sigma (St. Louis, MO).

Owing to the preparation conditions and intrinsic properties of the different SW mutant Mbs, these samples were initially obtained in various oxidation and ligation states (met, deoxy, oxy, carbonmonoxy). To ensure uniformity in the subsequent preparation of the deoxyMb samples, all of the SW proteins were treated as follows. The samples were first oxidized to the met form by adding an ∼3-fold excess of $K_3Fe(CN)_6$. The metMbs were flushed with N_2 for 30 min to remove CO or O_2. The samples were then solublized in phosphate buffer (pH 6.9, $I = 75$ mM), centrifuged to remove adventitious solid material, and passed through a Sephedex G-25 column using the same buffer as the elutant. Horse Mb was purified by standard procedures (*12*).

pH and GdmCl Jump Measurements. The deoxyMb samples for the pH and GdmCl jump experiments were prepared by equilibrating the purified metMbs (concentration ∼100 μM) at 4 °C in rigorously deoxygenated buffer (pH jumps, pH 6.9/$I = 75$ mM phosphate; GdmCl jumps, pH 8.0/$I = 50$ mM Tris) containing a slight excess of $Na_2S_2O_4$. The pH jumps were performed by rapidly injecting a 50-μL aliquot of the deoxyMb solution at the initial pH of 6.9 contained in an airtight syringe into an optical cuvette containing 250 μL of deoxygenated acetate buffer prepared to achieve a final pH of 3.2 and to maintain the ionic strength constant at $I = 75$ mM (final protein concentration, ∼16 μM). The GdmCl jumps were performed in a similar fashion with the final solution prepared to achieve a GdmCl concentration of 5.0 M and to maintain the pH at 8.0.

We emphasize the importance of maintaining uniformity in the ionic strength conditions for the pH jump experiments on the different samples because the rate of formation of the I′-intermediate is sensitive to this parameter (*25*). An ionic strength of 75 mM was chosen for the pH jump experiments because previous studies of native deoxyMb have shown that under these conditions the time evolution from the N-form to the I′-form is slow enough (seconds/minutes) to be easily measured in a conventional diode array spectrophotometer (*25*). In contrast, the rate of I′-intermediate formation dramatically accelerates/decelerates if the ionic strength is significantly increased/decreased during the pH jump (*25*).

The kinetic data were acquired by monitoring the absorption spectrum after sample injection using the software available with the spectrophotometer (vide infra). The time-zero data point was acquired ∼2 s after injection. Various

data collection times were used because the time evolution of the unfolding process varies by approximately 3 orders of magnitude for these proteins (vide infra).

Equilibrium pH and GdmCl Measurements. The deoxyMb samples for the equilibrium pH and GdmCl measurements were prepared generally as described above for the pH jump experiments with the following modifications. Previous studies have shown that the I′-intermediate forms in acidic medium only below pH ∼4.5 (*24*, *25*). Consequently, the equilibrium pH measurements were performed on samples prepared in acetate buffer (I = 50 mM) in the pH 4.5−2.9 range. For the equilibrium GdmCl studies, the samples were prepared in rigorously deoxygenated Tris buffer (pH 8.0, I = 50 mM) containing GdmCl at the desired concentration (0−6.0 M). The samples at the various pH values and GdmCl concentrations were examined using both absorption and RR spectroscopy. For both types of spectroscopic measurement, the deoxyMb sample was extracted with an airtight syringe and loaded into a cuvette (absorption studies) or a capillary tube (RR studies) under an inert atmosphere where the respective sample cell was also sealed. The sample concentrations were ∼20 and ∼100 μM for the absorption and RR studies, respectively.

Spectroscopic Methods. The absorption and RR spectra were obtained at ambient temperatures. The absorption spectra were acquired with a diode array spectrophotometer (HP8452). The RR spectra were acquired with a triple spectrograph (Spex 1877) equipped with a holographically etched 2400 groove/mm grating in the third stage. The excitation wavelengths were provided by the discrete outputs of a krypton ion (Coherent Innova 200-K3) laser. The scattered light was collected in a 90° configuration using a 50 mm f/1.4 Canon camera lens. A UV-enhanced charge-coupled device (CCD) was used as the detector (Princeton Instruments LN/CCD equipped with an EEV1152-UV chip). The laser power at the sample was 8 mW or less. The frequencies were calibrated using the known frequencies of indene and CCl_4. The spectral resolution was ∼2 cm^{-1}.

RESULTS

Kinetic and Equilibrium Studies of Acid-Induced Unfolding. pH jump experiments were conducted on all of the SW deoxyMbs. These experiments provided a relatively rapid procedure for determining whether the I′-intermediate was formed in the various mutants and/or whether the mutants exhibited any unusual spectral features under low pH unfolding conditions. On the basis of the results of the pH jump studies, certain SW deoxyMbs were selected for equilibrium pH studies.

(*A*) *pH Jump Studies*. Representative absorption spectra of wild-type deoxyMb obtained at selected times following a pH jump from 6.9 to 3.2 are shown in Figure 1 (left panel). The general features of the time evolution of the spectrum are similar to those we have previously reported for native deoxyMbs (*25*). In particular, the 434-nm Soret band characteristic of the N-form monotonically loses intensity and gradually shifts to the blue, yielding the 426-nm signature of the I′-intermediate. Subsequently, the spectrum evolves to the broad 383-nm absorption characteristic of the U′-form. The Soret absorption features of the H64A, H64V, H64Q, H64Q/L29F, L29V, L29F, V68T, and I107A deoxyMbs (not shown) also evolve in the same general fashion as those of the wild type, although not necessarily on the same time scale. This latter point is illustrated in Figure 2, which compares the spectra of wild-type and several mutant deoxyMbs obtained at times when the I′-intermediate makes approximately the largest contribution to the absorption spectrum.

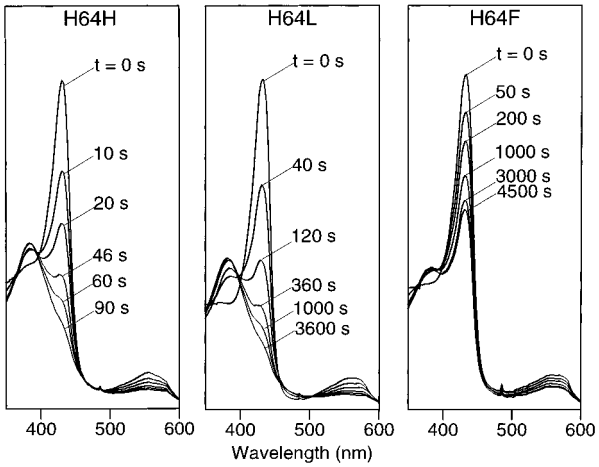

FIGURE 1: Time evolution of the absorption spectra of wild-type (H64H), H64L, and H64F SW deoxyMbs following the pH jump from 6.9 to 3.2. The ionic strengths of the initial and final solutions are both 75 mM.

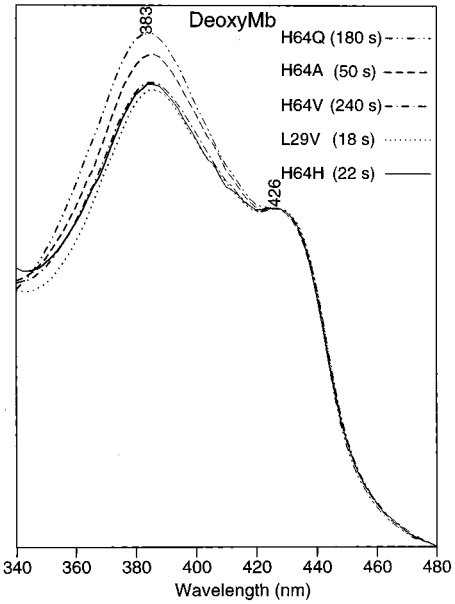

FIGURE 2: Comparison of the absorption spectra of various SW deoxyMbs after the pH jump. The traces shown are for the time when the I′-intermediate makes approximately the maximum contribution to the spectrum.

The behavior of the Soret absorption features of the H64L and H64F deoxyMbs following the pH jump is demonstrably different from that of the wild-type and the other mutant deoxyMbs. The time evolution of the absorption spectra of H64L and H64F are included in Figure 1 (middle and right panels, respectively). In the case of the H64L mutant, the spectrum evolves quite slowly and the 426-nm absorption feature characteristic of the I′-intermediate is never as prominent as that for the wild-type protein. For the H64F mutant, the spectral evolution is extraordinarily slow and the

Table 1: Comparison of I′-Intermediate Formation Kinetics, Deoxy/ApoMb Stability, Hemin Loss Rate, and Distal Heme Pocket Hydration State for Various Mbs

Mb	$\tau(pH_{I'-max})^a$ (pH 6.9 → 3.2) (s)	$pH_{I'-max}{}^a$	$\tau(GdmCl_{I'-max})^a$ (0 → 5.0 M) (s)	$GdmCl_{I'-max}{}^a$ (M)	$1/K_{N,I}K_{I,U}{}^b$	k_{-H} (pH 5)^c (h^{-1})	k_{-H} (pH 7)^c (h^{-1})	distal heme pocket water^d
native horse	35 ± 7[e]	~3.80[e]	33 ± 4[f]	~2.3[f]	*g*	2.5	*g*	yes
wild-type pig	*g*	*g*	*g*	*g*	600	1.0	0.01	yes
wild-type human	*g*	*g*	*g*	*g*	2 000	3	0.01	yes
wild-type SW	46 ± 20	~3.45	270 ± 53	~2.8	50 000	1.0	0.01	yes
H64A	99 ± 52	*g*	*g*	*g*	330 000	17	0.40	yes
H64V	246 ± 10	*g*	*g*	*g*	*g*	7.3	*g*	no
H64L	1096 ± 755	~3.20	57 ± 5	~3.0	740 000	11.0	0.20	no
H64F	>3000[h]	~3.10	293 ± 38	~3.3	1 600 000	4.8	0.01	no
H64Q	212 ± 55	~3.40	623 ± 180	~2.9	50 000	3.5	0.12	no/yes[i]
H64Q/L29F	174 ± 45	*g*	*g*	*g*	*g*	*g*	*g*	probably no[j]
L29V	25 ± 5	*g*	*g*	*g*	*g*	11.0	0.10	yes
L29F	20 ± 8	*g*	*g*	*g*	100 000	2.5	0.01	no
V68T	60 ± 23	~3.60	490 ± 17	~2.5	7 400	<0.1	<0.01	yes
I107A	15 ± 9	*g*	*g*	*g*	*g*	1.1	*g*	unknown

[a] $\tau(pH_{I'-max})$, $pH_{I'-max}$, $\tau(GdmCl_{I'-max})$, and $GdmCl_{I'-max}$ are the time (pH jump), equilibrium pH, time (GdmCl jump), and equilibrium GdmCl concentrations wherein the I′-intermediate makes approximately the maximum contribution to the absorption spectrum of deoxyMb (see text). The standard deviations in the jump experiments are based on 3−9 data sets. [b] ApoMb stability parameter (*9*). [c] Hemin loss rate from metMb (*8*). [d] See refs *12* and *29*−*37*. [e] Taken from ref *25*. [f] This study. [g] Value not determined. [h] The I′-intermediate for this mutant does not make an appreciable contribution to the absorption spectrum under the conditions of the pH jump experiments (see text). [i] The X-ray structure of deoxyH64Q shows no distal heme pocket water (*29*); however, the solution NMR spectrum indicates that water is present (*35*). [j] The presence of distal heme pocket water has not been explicitly determined for H64Q/L29F deoxyMb; however, the absence of water is inferred by analogy to L29F deoxyMb (*36*).

I′-intermediate does not appear to form under the conditions of the pH jump experiment. The stability of H64F deoxyMb is remarkable. Even 1 h after the jump to pH 3.2, a substantial amount of the protein remains in the N-form.

The times ($\tau(pH_{I'-max})$) at which the I′-intermediate makes approximately the maximum contribution to the absorption spectrum of the various deoxyMbs are summarized in Table 1. The $\tau(pH_{I'-max})$ values were obtained by averaging the results of the multiple kinetic runs. Inspection of these data leads to the following general characterization of the temporal features. (1) The $\tau(pH_{I'-max})$ values for the H64A, L29V, L29F, V68T, and I107A mutants are qualitatively similar to one another and similar to those of the wild type. The $\tau(pH_{I'-max})$ values do exhibit some variation among this group of deoxyMbs; however, these variations are generally within experimental error. (2) $\tau(pH_{I'-max})$ values for the H64V, H64Q, and H64Q/L29F deoxyMbs are qualitatively similar to one another and sufficiently longer than those of the proteins in the first group to be outside the range of experimental error. (3) The $\tau(pH_{I'-max})$ values for the H64L and H64F deoxyMbs are much longer than those for any of the other deoxyMbs. The $\tau(pH_{I'-max})$ value listed for H64F deoxyMb is clearly an underestimate given that the I′-intermediate does not form appreciably under the conditions of the pH jump experiment. For both the H64L and H64F mutants, the unfolding process is so slow under the conditions of the pH jump experiment that some oxidation to metMb occurs. Oxidation may be responsible for the relatively large errors observed in the $\tau(pH_{I'-max})$ value for the H64L mutant and the decay of the N-form of H64F without the apparent formation of the I′-intermediate. (4) Among the series of mutants containing a hydrophobic replacement at position 64, the $\tau(pH_{I'-max})$ values monotonically increase as the size of the residue increases: H64A, $\tau(pH_{I'-max})$ ~99 s < H64V, $\tau(pH_{I'-max})$ ~246 s < H64L, $\tau(pH_{I'-max})$ ~1096 s < H64F, $\tau(pH_{I'-max})$ > 3000 s.

(*B*) *Equilibrium pH Studies*. The unusual behavior observed for the H64L and H64F deoxyMbs in the pH jump experiments prompted us to examine the equilibrium pH behavior of these mutants. For comparison, equilibrium pH data were also obtained for the wild-type, H64Q, and V68T proteins. The absorption spectra of the wild-type, H64L, and H64F deoxyMbs at selected pH values are shown in Figure 3. The bottom trace for each deoxyMb shows the spectrum of the N-form of the protein. The second traces show the pH at which the Soret band begins to exhibit an appreciable shift to the blue. The third traces show the pH at which the 426-nm absorption characteristic of the I′-intermediate makes approximately the maximum contribution to the spectrum. The top traces show the pH at which the 383-nm absorption characteristic of the U′-form is the predominant contributor.

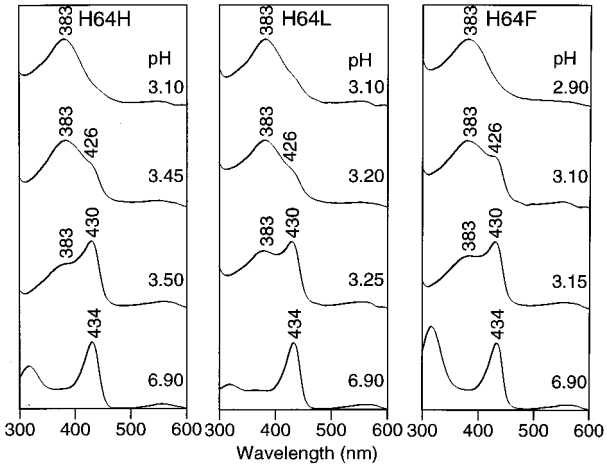

FIGURE 3: Absorption spectra of wild-type (H64H), H64L, and H64F SW deoxyMbs at selected pH values. The relative intensities of the different spectra do not represent the actual values but are scaled for pictorial clarity.

The data shown in Figure 3 indicate that the spectral features observed for the wild-type, H64L, and H64F mutants as a function of pH are qualitatively similar to one another and similar to those previously reported for native deoxyMbs

(*24*, *25*). In particular, the Soret maximum systematically shifts to the blue as the pH is lowered, yielding a 426-nm absorption feature characteristic of the I′-intermediate prior to progressing to a 383-nm absorption characteristic of the U′-form. The key difference in the spectra of the different deoxyMbs is that the pH ($pH_{I'-max}$) at which the 426-nm absorption feature makes approximately the maximum contribution to the spectrum monotonically shifts to lower values down the series wild type ($pH_{I'-max}$ ∼3.45)[2] > H64L ($pH_{I'-max}$ ∼3.20) > H64F ($pH_{I'-max}$ ∼3.10). On the other hand, the $pH_{I'-max}$ value for H64Q deoxyMb ($pH_{I'-max}$ ∼3.40) is nearly that same as for the wild-type protein, whereas the $pH_{I'-max}$ value for V68T is higher ($pH_{I'-max}$ ∼3.60). These $pH_{I'-max}$ values, in addition to that of horse deoxyMb ($pH_{I'-max}$ ∼3.80) (*25*), are included in Table 1.

The $pH_{I'-max}$ values obtained for the H64L and H64F deoxyMbs explain the anomalous behavior observed for these mutants in the pH jump experiments. In particular, the latter studies were performed with a jump to a final pH of 3.2. For the H64L mutant, this pH corresponds to a value approximately equal to $pH_{I'-max}$. For the H64F mutant, the final pH of 3.2 lies above $pH_{I'-max}$. Consequently, the conditions of the pH jump experiments would result in a relatively slow conversion of the H64L mutant to the I′-intermediate (compared with the time evolution expected for a jump to a final pH well below that at which the I′-intermediate is appreciably formed (*25*)). For the H64F mutant, little, if any, of the I′-intermediate would form, even at long times after the pH jump.

To confirm that the absorption features observed in the equilibrium pH experiments on the recombinant SW deoxyMbs are in fact due to the I′- and U′-intermediates previously characterized for native deoxyMbs (*24*, *25*), a series of RR studies were also performed on selected proteins. Representative Soret-excitation RR spectra of wild-type and H64L deoxyMbs are compared in Figures 4 (high-frequency region) and 5 (low-frequency region). The spectra shown in these figures were obtained at the same pH as that used to obtain the absorption spectra shown in Figure 3. The spectra of the N- and I′-forms were obtained with $\lambda_{ex} = 415.4$ nm, whereas that of the U′-form was obtained with $\lambda_{ex} = 356.4$ nm. A different exciting line was used for the latter form because the absorption maximum is significantly blue-shifted compared with those of the N- and I′-forms.

The data shown in Figures 4 and 5 reveal that the spectral signatures observed for the wild type and the H64L mutant as a function of pH are very similar to one another and similar to those previously reported for native deoxyMbs (*24*−*26*). The key features in the RR spectra are the ν_4 oxidation state marker band and the iron−histidine stretching mode, ν_{FeHis}, which are observed at 1354 and 219 cm^{-1}, respectively, for the N-form of deoxyMb (*14*, *15*). At lower pH values where the 426 nm absorbing species makes the maximum contribution to the absorption spectrum, the RR band due to ν_{FeHis} is absent from the RR spectrum, indicative

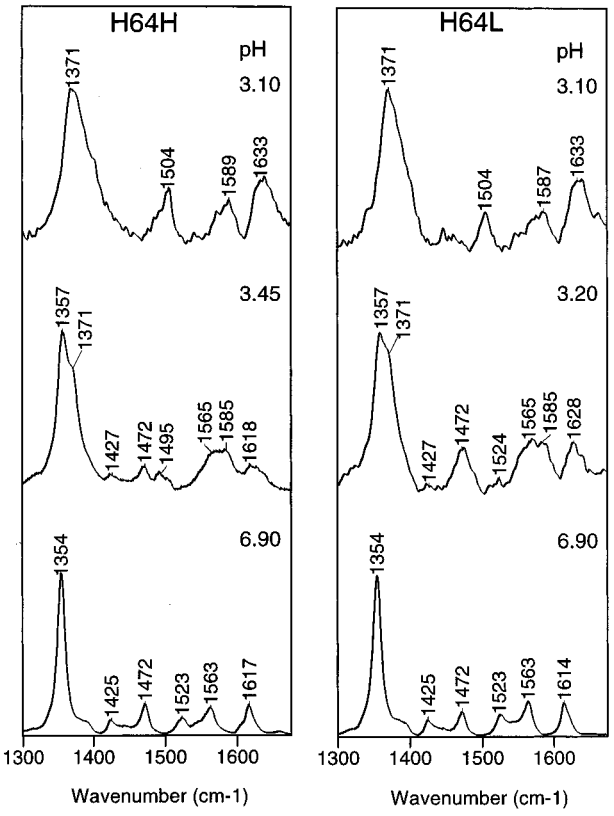

FIGURE 4: High-frequency regions of the Soret-excitation RR spectra of wild-type (H64H), and H64L SW deoxyMbs at selected pH values. The spectra at neutral and intermediate pH were acquired with $\lambda_{ex} = 415.4$ nm; the spectra at low pH were acquired with $\lambda_{ex} = 356.4$ nm.

of cleavage of the bond. In concert, the ν_4 band upshifts to ∼1357 cm^{-1}. Both of these RR spectral features are characteristic of the I′-intermediate (*24*). At lower pH values wherein the 383 nm absorbing species is the dominant contributor to the spectrum, the ν_4 band further upshifts to ∼1371 cm^{-1}. This spectral signature is characteristic of the U′-intermediate (*24*, *26*). Collectively, the RR data unambiguously confirm that the equilibrium pH intermediates observed for the recombinant wild-type and H64L deoxyMbs are the same as those observed for native deoxyMbs (*24*, *25*). Although the equilibrium pH studies have not been extended to all of the mutant deoxyMbs examined in the pH jump experiments, there is no reason to suspect that the 426 and 383 nm absorbing species observed for these mutants correspond to heme intermediates that are different from those characterized for native (*24*−*26*), wild-type, and the H64L proteins.

Finally, we note that no attempt was made to extract thermodynamic parameters from the equilibrium pH measurements. As we have previously discussed (*24*, *25*), the equilibrium concentrations of the various heme intermediates cannot be accurately assessed from the relative intensities of the Soret band features owing to the severe overlap of the absorptions of the N-, I′-, and U′-forms, exacerbated by the extremely broad features of the latter intermediate. Extraction of accurate concentrations from the RR spectra is even more problematic owing to the dependence of the RR intensity enhancement on the position of the exciting line with respect to the absorption maximum of a particular form of the protein. Regardless, the general trend wherein

[2] Previous studies on native SW deoxyMb indicate that the contribution of the I′-intermediate to the absorption spectrum maximizes at ∼pH 3.8 (*24*). However, these studies were conducted under significantly higher ionic strength conditions ($I > 100$ mM) than the present studies ($I = 50$ mM). Other work has shown that at low pH, the N-form is destabilized with respect to the I′-intermediate as the ionic strength increases (*25*).

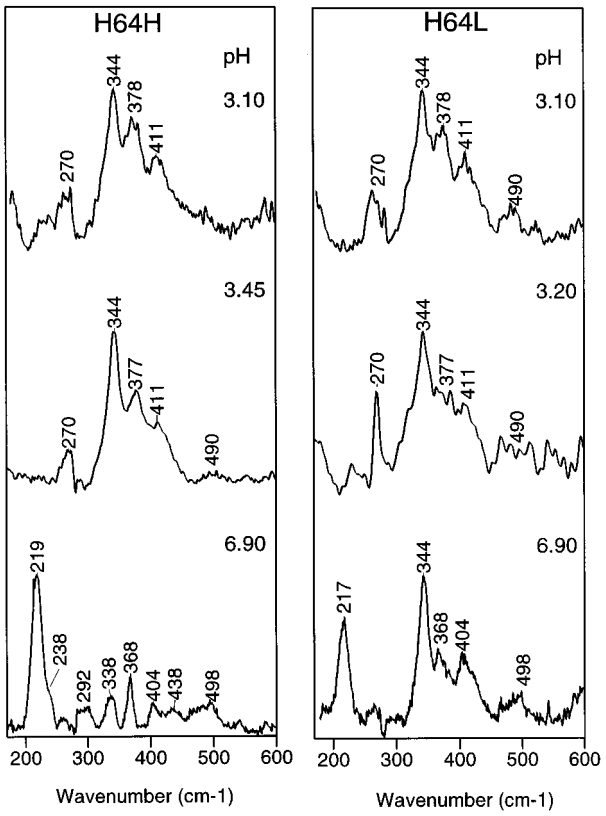

FIGURE 5: Low-frequency regions of the Soret-excitation RR spectra of wild-type (H64H), and H64L SW deoxyMbs at selected pH values. The spectra at neutral and intermediate pH were acquired with $\lambda_{ex} = 415.4$ nm; the spectra at low pH were acquired with $\lambda_{ex} = 356.4$ nm.

$pH_{I'-max}$ shifts to lower values down the series wild type > H64L > H64F is clearly evident in the data.

Kinetic and Equilibrium Studies of GdmCl-Induced Unfolding. To date, the formation of the I′-intermediate of deoxyMb has only been reported under acidic unfolding conditions (*21*−*25*). To gain further insight into the factors governing formation of this intermediate, a series of kinetic and equilibrium GdmCl unfolding studies was performed. These studies included the wild-type, H64Q, H64L, H64F, and V68T SW deoxyMbs as well as the native horse protein. The H64L and H64F mutants were chosen for their remarkable kinetic and equilibrium resistance to acidic unfolding. The H64Q mutant was chosen because of its similar apoprotein stability to that of the wild-type protein. The V68T protein was chosen because its apoprotein stability is much lower than that of wild type. Horse deoxyMb was included because I′-intermediate formation under both pH jump and equilibrium pH conditions has been thoroughly investigated for this protein (*25*).

(*A*) *GdmCl Jump Studies*. Representative absorption spectra of wild-type, H64L, and H64F deoxyMbs obtained at selected times following a GdmCl jump from 0 to 5.0 M are shown in Figure 6. Inspection of these data reveals that the general features observed in the time evolution of the spectra are similar to those observed for the pH dependence (cf. Figures 1 and 6). In particular, the 434-nm Soret band characteristic of N-form monotonically loses intensity and gradually shifts to the blue, yielding the 426-nm signature of the I′-intermediate. Subsequently, the spectrum evolves to the broad 383-nm absorption feature characteristic of the

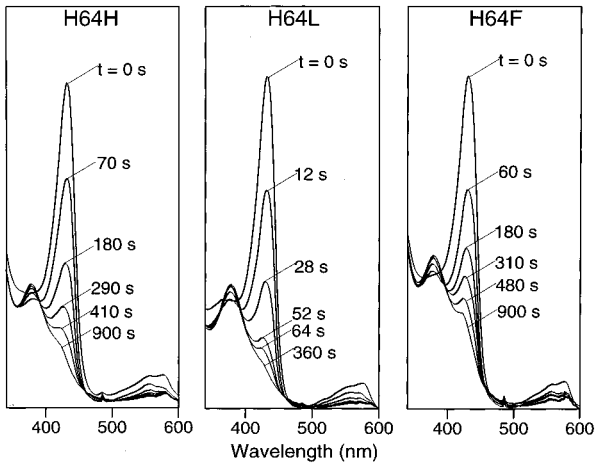

FIGURE 6: Time evolution of the absorption spectra of wild-type (H64H), H64L, and H64F SW deoxyMbs following the GdmCl jump from 0 to 5.0 M. The initial and final solutions are both pH 8.0.

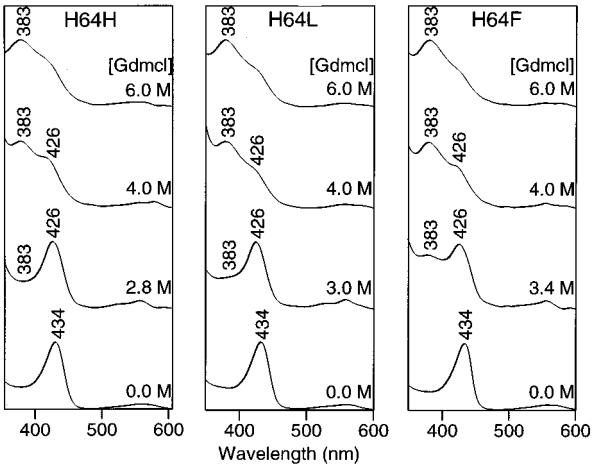

FIGURE 7: Absorption spectra of wild-type (H64H), H64L, and H64F SW deoxyMbs at selected GdmCl concentrations. The relative intensities of the different spectra do not represent the actual values but are scaled for pictorial clarity.

I′-form. The spectral features of H64Q and V68T SW and native horse deoxyMbs (not shown) evolve in a similar fashion. The key difference in the temporal behavior observed in the GdmCl versus pH jump experiments is that no correlation is apparent between the time ($\tau(GdmCl_{I'-max})$) when the I′-intermediate maximizes and the polarity of the position 64 residue. The $\tau(GdmCl_{I'-max})$ values for all the proteins investigated are included in Table 1.

(*B*) *Equilibrium GdmCl Studies*. The absorption spectra of the wild-type, H64L, and H64F deoxyMbs at selected GdmCl concentrations are shown in Figure 7. Inspection of these data (and those obtained at other GdmCl concentrations (not shown)) reveals that the trends observed in the absorption spectra again generally parallel those described above and previously reported for the equilibrium pH dependence of the spectra (*25*). In particular, as the GdmCl concentration increases, the 434-nm Soret band characteristic of the N-form gradually loses intensity and blue shifts. With GdmCl concentrations in the 2.8−3.5 M range, absorption features at 426 and 383 nm are apparent for both the wild-type and the two mutant deoxyMbs, consistent with formation of the I′- and U′-intermediates, respectively.

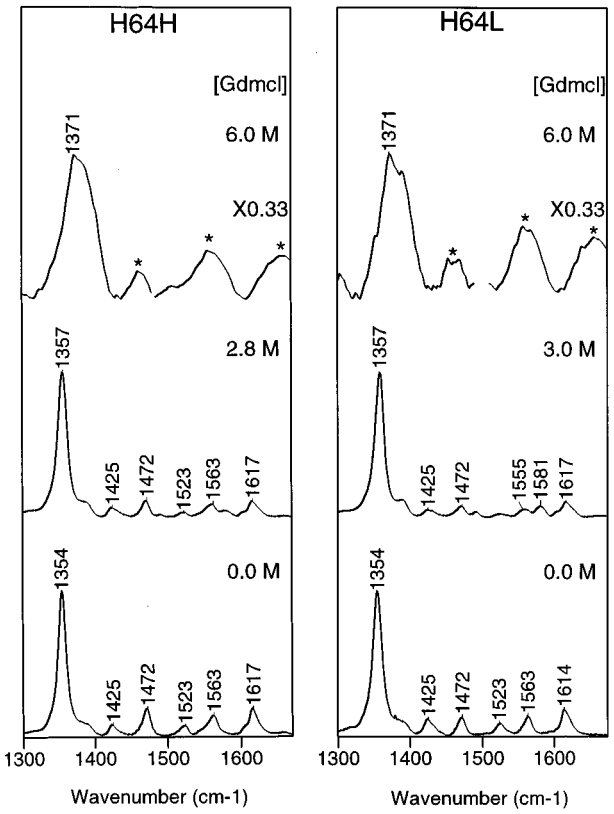

FIGURE 8: High-frequency regions of the Soret-excitation wild-type (H64H), and H64L SW deoxyMbs at selected GdmCl concentrations. The spectra at zero and intermediate GdmCl concentrations were acquired with $\lambda_{ex} = 415.4$ nm; the spectra at high GdmCl concentrations were acquired with $\lambda_{ex} = 356.4$ nm. The bands marked by asterisks are due to GdmCl.

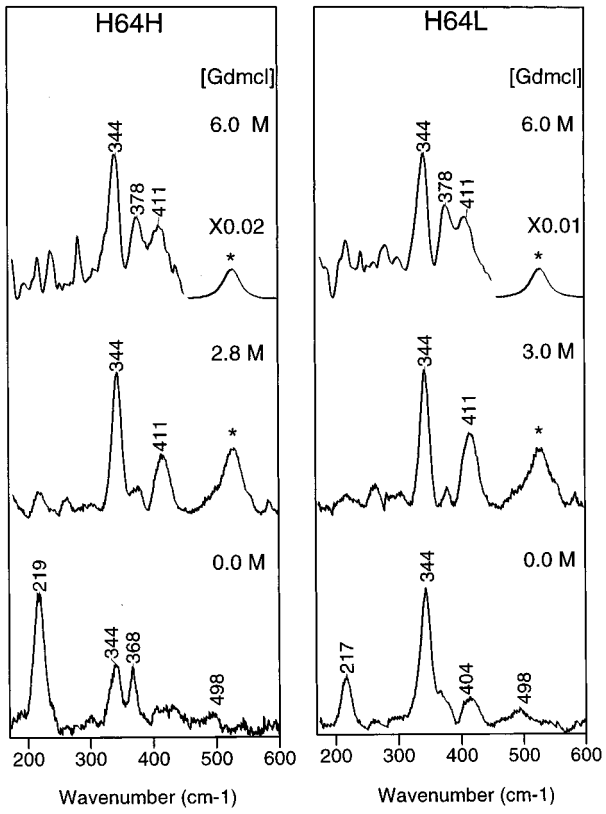

FIGURE 9: Low-frequency regions of the Soret-excitation wild-type (H64H), and H64L SW deoxyMbs at selected GdmCl concentrations. The spectra at zero and intermediate GdmCl concentrations were acquired with $\lambda_{ex} = 415.4$ nm; the spectra at high GdmCl concentrations were acquired with $\lambda_{ex} = 356.4$ nm. The bands marked by asterisks are due to GdmCl.

The I′-intermediate appears to form more cleanly in the GdmCl titrations, as is evidenced by the relatively sharp 426-nm Soret features observed for the wild-type and H64L proteins compared with those seen in the pH titration experiments (cf. Figures 3 and 7). The sharp appearance of the Soret band of the I′-intermediate appears to be due to a smaller rate of autoxidation at pH 8.0. As the GdmCl concentration increases further, the 426-nm Soret band of the I′-intermediate is attenuated and the 383-nm band of the U′-form gains additional intensity. As shown in Table 1, the GdmCl concentration ($GdmCl_{I'-max}$) causing the maximum amount of I′-intermediate monotonically shifts to higher values for the series wild type/H64Q ($GdmCl_{I'-max}$ ∼2.8−2.9 M) < H64L ($GdmCl_{I'-max}$ ∼3.0 M) < H64F ($GdmCl_{I'-max}$ ∼3.3 M). The $GdmCl_{I'-max}$ values for V68T SW and horse deoxyMbs are both considerably lower ($GdmCl_{I'-max}$ ∼2.5 and ∼2.3 M, respectively) than that for wild-type SW deoxyMb. This trend parallels that observed in the equilibrium pH titrations.

RR spectra were obtained for the wild-type and H64L SW deoxyMbs and the native horse protein again to confirm that the absorption features observed in the equilibrium GdmCl experiments are in fact due to the I′- and U′-intermediates. Representative Soret-excitation RR spectra of the wild-type and H64L deoxyMbs are compared in Figures 8 (high-frequency region) and 9 (low-frequency region). The spectra shown in these figures were obtained at the same GdmCl concentrations used to obtain the data shown in Figure 7. Comparison of these spectra with those obtained in the equilibrium pH studies (Figures 4 and 5) reveals that the characteristics of the I′-intermediate (ν_{Fe-His} is absent from the spectrum; ν_4 at ∼1357 cm^{-1}) and the U′-intermediate (ν_4 at ∼1371 cm^{-1}) are clearly apparent under conditions in which the 426 and 383 nm absorbing species make dominant contributions to the absorption spectrum. The RR spectra of native horse deoxyMb (not shown) are similar. Collectively, the absorption and RR spectra indicate that GdmCl-induced denaturation and low pH unfolding of deoxyMb proceed through the same heme intermediates.

DISCUSSION

The results summarized in Table 1 provide new insights into the factors that govern the lability of the iron−histidine bond and the overall stability of deoxyMb. The four key observations are as follows. (1) None of the distal heme pocket mutations investigated alter the nature of the deoxyheme intermediates that are formed under low pH unfolding conditions. (2) The unfolding of deoxyMb under high GdmCl conditions proceeds through the same heme intermediates as those which occur under low pH conditions. (3) The rate of the iron−histidine bond cleavage in acidic medium is dramatically slowed when large hydrophobic residues (Leu and Phe) are substituted for the native distal histidine residue. (4) Mutant deoxyMbs containing apolar residues at position 64 exhibit enhanced equilibrium resistance to iron−histidine bond cleavage under both low pH and high GdmCl conditions. These results allow the development of structural mechanisms for the denaturation

of deoxyMb that are distinct from those that apply to the denaturation of metMb and may be important for understanding the expression of recombinant myoglobins and hemoglobins.

The Rate and Extent of Acid Unfolding of DeoxyMb Correlate Inversely with Apoglobin Stability. Hargrove and Olson systematically examined the factors that govern the stability of holo aquometMb under physiological conditions (*5*). In general, the equilibrium constant describing the denaturation of metMb correlated more directly with the rate of hemin dissociation than with either the individual or the composite unfolding constant for the corresponding apoproteins. Because formation of the I′-intermediate during the denaturation of deoxyMb involves breakage of the iron−proximal histidine bond, we initially thought that there would be a correlation between the rate and extent of formation of this ferrous intermediate and the rate of hemin dissociation, $k_{-H,}$ from the corresponding metMb protein. As shown in Table 1, there is little correlation between k_{-H} and either $\tau(pH_{I'-max})$, $pH_{I'-max}$, $\tau(GdmCl_{I'-max})$, or $GdmCl_{I'-max}$. For example, H64L metMb loses hemin ∼10−20 times more rapidly than wild-type metMb (*8*), but the mutant deoxyMb forms the I′-intermediate 20 times more slowly and requires 0.2 pH unit more acidic conditions than the wild-type ferrous protein to achieve the maximum amount of this species at equilibrium. Similarly, the $GdmCl_{I'-max}$ value for H64L deoxyMb is 0.2 M greater than for wild-type.

Because the I′-intermediate is a pentacoordinate aquoheme complex (*25*), we looked for a correlation between the presence of a distal heme pocket water molecule in the crystal structure of the various deoxyMbs and the rate and extent of denaturation. With one exception, there is a correlation between a rapid rate of I′-intermediate formation under acidic conditions and the presence of a discrete internal water molecule (Table 1). The L29F mutant is the major exception. The I′-intermediate forms rapidly for this deoxyMb despite the absence of a distal heme pocket water molecule (*36*). However, it is difficult to quantitate this effect because the equilibrium constant for water binding to deoxyMb cannot be measured. Moreover, the correlation between rapid I′-intermediate formation and the presence of heme pocket water does not extend to GdmCl-denaturing conditions. For example, the $\tau(GdmCl_{I'-max})$ value for H64L deoxyMb is ∼5 times smaller than for wild-type protein, opposite the trend observed for acid unfolding.

Unexpectedly, there is a strong inverse correlation between the extent of I′-intermediate formation and the stability of the corresponding apoglobin. The apoprotein stabilities, $1/K_{N,I}K_{I,U}$, reported in Table 1 were calculated from the unfolding equilibrium constants ($K_{N,I}$ and $K_{I,U}$) determined by Hargrove et al. (*9*). The correspondence between I′-intermediate formation and apoglobin stability is clearly evident in both the low pH and high GdmCl denaturing data and applies to sperm whale as well as to other mammalian Mbs. In particular, the $pH_{I'-max}$ and $GdmCl_{I'-max}$ values monotonically shift to lower and higher values, respectively, as the overall apoprotein stability parameter, $1/K_{N,I}K_{I,U}$, increases. As shown in Table 1, an ∼0.7 pH unit decrease and an ∼1 M GdmCl increase are required to cleave the iron−histidine bond in H64F deoxyMb, whose apoglobin is the most stable ($1/K_{N,I}K_{I,U}$ ∼ 1 600 000) compared to that of native noncetacean myoglobin ($1/K_{N,I}K_{I,U}$ ∼ 600−2000). In the case of acid (but not GdmCl) denaturation, there is also a rough correlation between the time for maximum I′-intermediate formation and apoglobin stability, particularly for the series of position 64 mutants. For example, $\tau(pH_{I'-max})$ is ∼50 s for wild-type SW deoxyMb with an apoglobin stability of ∼50 000 and increases almost 60-fold to >3000 s for H64F deoxyMb, which has an apoprotein stability of ∼1 600 000.

Mechanism for Ferrous Iron−Histidine Bond Cleavage and Heme Loss in DeoxyMb. The kinetic and equilibrium behavior of the different deoxyMbs under acidic and high GdmCl denaturing conditions suggests that global unfolding of the protein is required for cleavage of the ferrous iron−histidine bond and heme loss from deoxyMb. This process is facilitated by the distal histidine, which tends to hydrate the heme pocket. This view is supported by the observation that large apolar residues, such as Leu and Phe, at position 64 inhibit denaturation, presumably by making the heme pocket more anhydrous, which in turn stabilizes the globin structure and prevents ferrous iron−histidine bond cleavage. Placing a Gln residue at position 64 has little effect on either $pH_{I'-max}$ or $GdmCl_{I'-max}$ because the polarity of this residue is similar to that of the naturally occurring histidine.

The fact that the same heme intermediates are formed under both low pH and high GdmCl unfolding conditions indicates that iron−histidine bond cleavage, even in an acidic environment, is not driven by protonation of the proximal histidine residue. Instead, severance of this linkage is a more general consequence of protein unfolding. This behavior can be rationalized in terms of the binding affinity of nitrogenous bases to heme (*38*−*40*). In particular, the affinity of heme for a single imidazole is very weak, whereas the affinity for the second ligand is very great. As a result, imidazole binding is completely cooperative (*n*-values ∼ 2), making the dissociation constant for the first base indeterminate but at least 10-fold greater than the concentration of free base at half-saturation (≫10^{-3}−10^{-4} M) in most titration experiments with heme model complexes (*40*). In the present study, the concentration of deoxyMb is ∼20−100 μM; consequently, ligation of a single histidine will not occur unless the protein is properly folded to allow specific heme binding and proper orientation of the proximal histidine residue (*5*). Accordingly, the proximal histidine does not have to be protonated to prevent ligation to the heme. Unfolding of the protein is sufficient because the nonspecific base affinity is too small to allow chelation at such low histidine and heme concentrations.

Although protonation of the proximal histidine (His 93) is not required for iron−histidine bond cleavage in deoxyMb, protonation of the distal histidine (His 64) under acidic conditions facilitates further hydration of the heme pocket and unfolding of the protein. Crystallographic studies of Mb at low pH have shown that protonation of the distal histidine causes the imidazole side chain to rotate out of the heme pocket into the bulk solvent, creating a direct channel for the entry of water into the center of the protein (*41*). The kinetics of this process might be expected to be similar for all mutant proteins containing a distal histidine residue barring new specific interactions between His 64 and the replacement residue at some other position. This view would explain why all naive/wild-type deoxyMbs and mutants with replacements at positions other than 64 exhibit similar, rapid rates of I′-intermediate formation. The non-native residues

introduced at positions 29, 68, and 107 cannot block the channel opened by movement of the distal histidine side chain out into the bulk solvent. On the other hand, mutants with apolar amino acids at position 64 would be expected to exhibit very different kinetics because movement of a hydrophobic residue into solvent is energetically unfavorable. This interpretation explains why the I′-intermediate formation rate is very slow for the H64A, H64V, H64L, and H64F mutants and why the rate generally decreases as the size of hydrophobic residue increases. The relatively slow rates observed for H64Q and H64Q/L29F deoxyMb also support the solvation kinetic mechanism for acid denaturation. Rotation of Gln 64 into the solvent is less favorable than for His because the amino acid side chain cannot be protonated. As a result, the rate of I′-intermediate formation for deoxyMb containing the large, but polar, Gln residue is similar to that observed for deoxyMb containing the smaller, but apolar, Val residue.

Finally, the kinetics of I′-intermediate formation under high GdmCl denaturing conditions is quite different from that observed under acidic conditions. Under the GdmCl denaturing conditions at pH 8.0, the distal histidine is not protonated. Hence, there is no obvious mechanism by which His 64, but not Gln 64, can facilitate hydration of the heme pocket. Consistent with this idea, wild-type SW deoxyMb exhibits a significantly slower rate of I′-intermediate formation under GdmCl denaturing conditions than is observed for acid conditions. However, the time for maximum I′-intermediate formation by wild-type deoxyMb (∼270 s) is ∼4 times longer than that for the H64L protein (∼60 s). Curiously, the times for native horse protein are similar for GdmCl and acid denaturing conditions (∼33 and ∼35 s, respectively; Table 1). The absence of a trend in the rate data precludes development of a model for GdmCl-induced denaturation.

CONCLUSIONS

Global solvation of the distal heme pocket appears to be the key element in the cleavage of the iron−histidine bond in deoxyMb under both low pH and high concentrations of GdmCl. Iron−histidine bond cleavage does not appear to be driven by protonation of the proximal histidine ligand even at low pH. Instead, the process is mediated by global unfolding of the protein and hydration of the heme pocket. Mutants of deoxyMb containing hydrophobic amino acids at position 64 are unusually resistant to heme pocket solvation and, hence, iron−histidine bond cleavage. This resistance to internal solvation is also reflected in significantly higher stability of the corresponding apoglobins. Both of these features are consistent with the ability to express large amounts of these mutants in *Escherichia coli* (*9*). The high affinity for heme shown by deoxyMb compared to that for hemin by metMb is due to the much stronger ferrous iron−histidine bond. As a result, the loss of heme from deoxyMb requires unfolding of the protein, exposing the pentacoordinate heme complex to solvent. This exposure results in ferrous iron−histidine bond cleavage because the equilibrium constant for the binding of a single imidazole base is quite small in the absence of protein steric constraints which confine the base near the fifth coordinate position of the heme iron atom.

The correlations in Table 1 show that enhancing apoglobin stability also enhances the resistance of deoxyMb to denaturation. This result helps to explain the correlation between apoglobin stability and holoprotein expression yields in *E. coli* reported by Hargrove et al. (*9*). Even in the presence of oxygen, the cytoplasm of the bacterium is reducing, and in the packed cells, substantial amounts of deoxyMb are present. These results also provide insights for the design of extracellular heme proteins for use as O_2 delivery pharmaceuticals. The success of these proteins hinges on their ability to exhibit the requisite O_2 binding characteristics, to discriminate against inhibitory ligands and signal molecules (such as CO and NO), be stable under adverse conditions (such as acidic pH), and to be expressed in high yield in bacterial or yeast systems.

REFERENCES

1. Dickerson, R. E., and Geis, I. (1983) *Hemoglobin*, Benjamin/Cummings, Menlo Park, CA.
2. Hargrove, M. S., Barrick D., and Olson, J. S. (1996) *Biochemistry 35*, 11293−11299.
3. Crumpton, M. J., and Polson, A. (1965) *J. Mol. Biol. 11*, 722−729.
4. Kawahara, K., Kirshner, A. G., and Tanford, C. (1965) *Biochemistry 4*, 1203−1213.
5. Hargrove, M. S., and Olson, J. S. (1996) *Biochemistry 35*, 11310−11318.
6. Griko, Y. V., Privalov, P. L., Venyaminov, S. Y., and Kutyshenko, V. P. (1988) *J. Mol. Biol. 202*, 127−138.
7. Hughson, F. M., Wright, P. E., and Baldwin, R. E. (1990) *Science 249*, 1544−1548.
8. Hargrove, M. S., Wilkinson, A. J., and Olson, J. S. (1996) *Biochemistry 35*, 11300−11309.
9. Hargrove, M. S., Krzywda, S., Wilkinson, A. J., Dou, Y., Ikeda-Saito, M., and Olson, J. S. (1994) *Biochemistry 33*, 11767−11775.
10. Bunn, H. F., and Jandel, J. H. (1968) *J. Biol. Chem. 243*, 465−475.
11. Allis, J. W., and Steinhardt, J. (1970) *Biochemistry 9*, 2286−2293.
12. Antonioni, E., and Brunori, M. (1971) *Hemoglobin and Myoglobin in Their Reaction with Ligands*, American Elsevier, New York.
13. Makinen, M. W., and Churg, A. K. (1983) In *Iron Porphyrins* (Lever, A. P. B., and Gray, H. B., Eds.) Part I, pp 141−236, Addison-Wesley, Reading, MA.
14. Choi, S., Spiro, T. G., Langry, K. C., Smith, K. M., Budd, D. L., and La Mar, G. N. (1982) *J. Am. Chem. Soc. 104*, 4345−4351.
15. Hu, S., Smith, K. M., and Spiro, T. G. (1996) *J. Am. Chem. Soc. 118*, 12638−12646.
16. Acampo, G., and Hermans, J., Jr. (1967) *J. Am. Chem. Soc. 89*, 1543−1547.
17. Puett, D. (1973) *J. Biol. Chem. 248*, 4623−4634.
18. Bismuto, E., Colonna, G., and Irace, G. (1983) *Biochemistry 22*, 4165−4170.
19. Irace, G., Bismuto, E., Savy, F., and Colonna, G. (1986) *Arch. Biochem. Biophys. 244*, 459−469.
20. Privalov, P. L., Griko, Y. V., Venyaminov, S. Y., and Kutyshenko, V. P. (1986) *J. Mol. Biol. 190*, 487−498.
21. Giacometti, G. M., Traylor, T. G., Ascenzi, P., Brunori, M., and Antonini, E. (1977) *J. Biol. Chem. 252*, 7447−7448.
22. Coletta, M., Ascenzi, P., Traylor, T. G., and Brunori, M. (1985) *J. Biol. Chem. 260*, 4151−4155.
23. Han, S., Rousseau, D. L., Giacometti, G., and Brunori, M. (1990) *Proc. Natl. Acad. Sci. U.S.A. 87*, 205−209.
24. Palaniappan, V., and Bocian, D. F. (1994) *Biochemistry 33*, 14264−14274.
25. Tang, Q., Kalsbeck, W. A., and Bocian, D. F. (1997) *Biospectroscopy 3*, 17−29.

26. Sage, J. T., Morikis, D., and Champion, P. M. (1991) *Biochemistry 30*, 1227−1237.
27. Takano, T. (1977) *J. Mol. Biol. 110*, 537−568.
28. Phillips, S. E. V. (1981) Brookhaven Protein Data Bank, Brookhaven, New York, PDB number 1MBD.
29. Quillin, M. L., Arduini, R. M., Olson, J. S., and Phillips, G. N., Jr. (1993) *J. Mol. Biol. 234*, 140−155.
30. Giacometti, G. M., Ascenzi, P., Brunori, M., Rigatti, G., Giacometti, G., and Bolognesi, M. (1981) *J. Mol. Biol. 151*, 315−319.
31. Morikis, D., Champion, P. M., Springer, G. A., Egeberg, K. D., and Sligar, S. G. (1990) *J. Biol. Chem. 265*, 12143−12145.
32. Ikeda-Saito, M., Hori, H., Andersson, L. A., Prince, R. C., Pickering, I. J., George, G. N., Saunders, C. R., II, Lutz, R. S., McKelvey, E. J., and Mattera, R. (1992) *J. Biol. Chem. 267*, 23641−23647.
33. Christian, J. F., Unno, M., Sage, T. J., Champion, P. M., Chien, E., and Sligar, S. G. (1997) *Biochemistry 36*, 11198−11204.
34. Rajarathnam, K., La Mar, G. N., Chiu, M. L., Sligar, S. G., Singh, J. P., and Smith, K. M. (1991) *J. Am. Chem. Soc. 113*, 7886−7892.
35. La Mar, G. N., Dalichow, F., Zhao, X., Dou, Y., Ikeda-Saito, M., Chiu, M. L., and Sligar, S. G. (1994) *J. Biol. Chem. 47*, 29629−29635.
36. Quillin, M. L. (1995) Ph.D. Thesis, Rice University, Houston, TX.
37. Smerdon, J. S., Dodson, G. G., Wilkinson, A. J., Gibson, Q. H., Blackmore, R. S., Carver, T. E., and Olson, J. S. (1991) *Biochemistry 30*, 6552−6560.
38. Cole, S. J., Curthoys, G. C., and Magnusson, E. A. (1970) *J. Am. Chem. Soc. 92*, 2991−2996.
39. Cole, S. J., Curthoys, G. C., and Magnusson, E. A. (1971) *J. Am. Chem. Soc. 93*, 2153−2158.
40. Brault, D., and Rougee, M. (1974) *Biochemistry 13*, 4591−4596.
41. Yang, F., and Phillips, G. N., Jr. (1996) *J. Mol. Biol. 256*, 762−774.

BI9729413